Spectrochimica Acta Part A 78 (2011) 967–980

Contents lists available at ScienceDirect

Spectrochimica Acta Part A: Molecular and Biomolecular Spectroscopy

journal homepage: www.elsevier.com/locate/saa

Vibrational spectroscopic study on 2-[2-(4-dipropylamino-phenyl)-vinyl]-1,3,3-trimethyl-3H-indolium chloride

Ferenc Billes[a,b,*], András Szabó[c], Yaroslav Studenyak[d]

[a] Department of Physical Chemistry and Material Science, Budapest University of Technology and Economics, Budafoki út 8, H-1521 Budapest, Hungary
[b] Institute for Chemical Technology and Analytik, Vienna University of Technology, Getreidemarkt 9/163, A-1060 Vienna, Austria
[c] Department of Organic Chemistry and Technology, Budapest University of Technology and Economics, Budafoki út 8, H-1521 Budapest, Hungary
[d] Department of Analytical Chemistry, Uzhorod National University, vul. Pidhirna 46, Uzhorod UA-88000, Ukraine

ARTICLE INFO

Article history:
Received 8 June 2010
Accepted 6 December 2010

Keywords:
Styryl dye
Vibrational spectra
Quantum chemistry
Normal coordinate analysis
Spectrum simulation
Solvent effect

ABSTRACT

A new styryl dye were prepared, 2-[2-(4-dipropylamino-phenyl)-vinyl]-1,3,3-trimethyl-3H-indolium chloride (DPPTVI) chloride. Its infrared and Raman were measured. Quantum chemical calculations were computed for both the isolated and the solute cation. Optimized geometry, atomic net charges were calculated. The calculated vibrational frequencies were scaled to the experimental ones. Only 12 scale factors were used for the scaling of 174 vibrational modes. Based on these results, normal coordinate analysis were carried out for both the isolated and the solute cations. Infrared and Raman spectra were simulated. The results for the isolated and the solute cations were compared.

1. Introduction

2-[2-(4-Dipropylamino-phenyl)-vinyl]-1,3,3-trimethyl-3H-indolium chloride (DPPTVI chloride) is a new dye that seems very suitable for analytical applications through complexation. In this way it can be applied for quantitative analytic determination of organic and inorganic ions.

The literature of styryl dyes is very wide. They are applied for several purposes. Deligeorgiev et al. [1] in their recent review about the synthesis and application of styryl dyes during last 15 years mention several applications of these dyes, e.g. in optics and laser technique. They are applied in the medical practice [2,3], and as fluorescent reagents [2,4].

One of the broad spheres of application of styryl dyes is analytical chemistry. Namely, several styryl dyes contain polar groups, which are capable for complexation. The complexation process was studied by Druzhinin et al. [5].

The choice of the appropriate compounds depends on their acid–base properties. Lehman et al. [6] synthesized and studied these properties of some amphiphylic acidichromic hydroxystilbazolium dyes. Osman et al. [7] synthesized oxazine methine cyanine dyes with one and two vinylydene groups and similarly investigated also their acid–base properties. Balogh et al. [8] dealt with the pH dependence of Cation Violet. Andruch and coworkers [9] studied the structure and acid–base properties of the (2-[2-4(-methoxy-phenylamino)-vinyl]-1,3,3-trimethyl-3H-indolium-ion.

Complexation is applied first of all for the determination of cations. Determination of magnesium [10–12], mercury, lead [13], cadmium [13,14] calcium, strontium and barium [11], manganese [15] is reported. Selenium can be analyzed through an indirect way, by applying chemical reactions [16]. The determination of nitrophenols is based on their interaction with the Astrazon Violet 3R dye [17]. Boron is analyzable after its conversion into boron tetrafluoride anion [18].

2. Experimental

2.1. Synthesis

Synthesis of the styryl dye, 2-[2-(4-dipropylaminophenyl)-1-ethenyl]-1,3,3-trimethyl-3*H*-indolium chloride was achieved through condensation of equimolar amounts of 4-(dipropylamino)benzaldehyde and proper quaternary ammonium salt (Fisher base) in an acetic anhydride (with addition of triethylamine) as depicted in the Scheme 1.

Method of synthesis: A mixture containing salt of Fisher base (1.048 g, 5 mmol), 4-(dipropylamino)benzaldehyde (1.025 g, 5 mmol), acetic anhydride (3 ml) and 2 drops of triethylamine was

* Corresponding author at: Department of Physical Chemistry and Material Science, Budapest University of Technology and Economics, Budafoki út 8, H-1521 Budapest, Hungary. Tel.: +36 1 463 1267; fax: +36 1 463 3767.
E-mail address: fbilles@mail.bme.hu (F. Billes).

1386-1425/$ – see front matter © 2010 Elsevier B.V. All rights reserved.
doi:10.1016/j.saa.2010.12.007

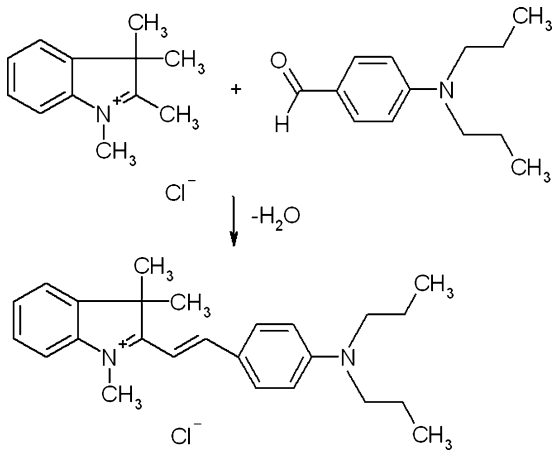

Scheme 1. Synthesis strategy.

heated under reflux for 5 min. After cooling, the dark crystals with metallic sheen were filtered, washed with diethyl ether and dried. The subsequent purification of the synthesized dye was done by re-crystallization from methanol.

2.2. Spectroscopic measurements

The infrared spectra were recorded on a Bruker tensor 37 spectrometer in KBr disks, with DTGS detector, in the 4000–400 cm^{-1} region.

The Raman spectra were measured applying a Jobin-Yvon Horiba LabRAM spectrometer, in the 4000–200 cm^{-1} region. A Wright CCD (256 × 1024) detector was used. The 785 nm laser band was found as the best one for excitation of the spectra. Namely, the sample showed strong fluorescence at 532 nm or 633 nm excitation. The integration time was changed from 60 s to 600 s, depending on the spectral region; the SNR was under these conditions not satisfactory in the CH stretching region, because of the low quantum efficiency of CCD for NIR photons. The spectra were base line corrected.

Strong fluorescence of the compound was observed in DMSO solution. The observed emission maximum was at 611 m [19].

3. Calculations

Quantum chemical calculations were carried out. The DFT method with the B3P86 hybrid functional [20,21] and the 6-31G* basis set was chosen for the computations, using the Gaussian 03 program package [22]. The first step of the calculations produced the optimized molecular geometry, the NBO and Mulliken's atomic net charges. The second step gave us the unscaled vibrational frequencies, infrared and Raman intensities with their depolarization factors and the vibrational force constants.

The inverted kinetic energy matrix (G matrix) was calculated using the optimized molecular geometry and the atomic mass values. The quantum chemical results contain the force constant matrices (F matrix) in atomic units. These were transformed into SI units and into the internal coordinate system defined by us. The force constants (the full F matrix) were scaled to the experimental frequencies through fitting the GF matrix eigenvalues to the experimental frequency data with optimization. Since the cation of the DPPTVI molecule contains 60 atoms, 174 internal coordinates were defined. This is also the magnitude of the scaling. However, only 12 independent scale factors were necessary for the scaling, providing that chemically similar coordinates can have the same scale factor. The eigenvectors of the GF matrix were used for the potential energy distribution (PED) matrix. The weights of the chemically similar coordinates were summed up. Based on the scaled calculated frequencies and the corresponding calculated intensities the infrared and Raman spectra were simulated.

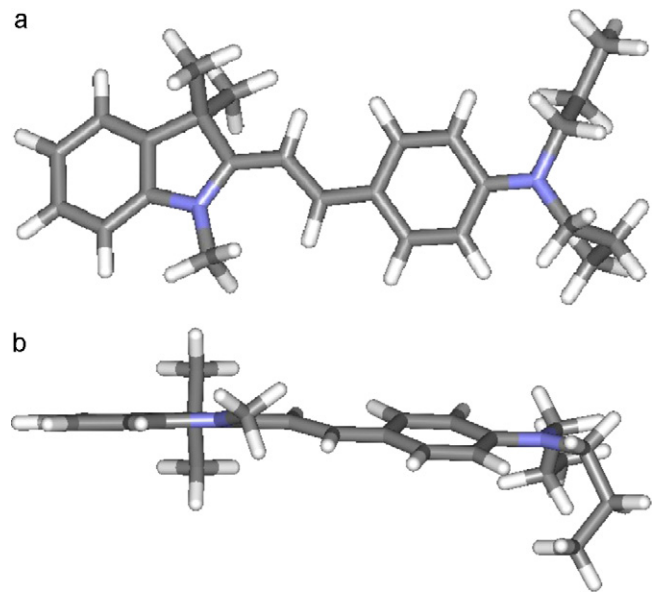

Fig. 1. (a) Optimized geometry of the DPPTVI cation, view a. (b) Optimized geometry of the DPPVTI cation, view b.

Home-made programs were applied for the elaboration of the quantum chemical results. This comprises calculation of the inverse kinetic energy (G) matrix, transformation of the calculated force constants into the field of the defined internal coordinates, normal coordinate analysis including the calculation of the potential energy distributions and simulation of the vibrational spectra.

In order to reveal the effect of water as a solvent on the DPPVTI properties we simulated the properties of this molecule in aqueous solution. Namely, as an analytical reagent, DPPVTI is used in aqueous solution. The polarized continuum model (PCM) [23–25] was applied. For the molecule in solution the same quantum chemical calculations were carried out as those for the isolated one. The further application of the quantum chemical data was also similar. The optimized scale factors were transferred from the isolated DPPTVI to the solute one. The results of the two calculations were compared.

The overlapping bands were resolved by deconvolution [26].

4. Results and discussion

4.1. Molecular geometry

DPPTVI can have several conformers since quasi free rotations are possible around some single bonds. We have performed calculations for one of the possible DPPTVI configurations.

Fig. 1 introduces the calculated optimized geometry of the DPPTVI cation in two views (*a* and *b*). Although there is a conjugative coupling possible between the phenyl and the indole rings, the two rings are not coplanar. The conjugation can spread through an N–C bond of the pyrrolidnium ring and the C=C bond of the vinyl group (see also Table 1). The numbering of the DPPTVI atoms is presented in Fig. 2.

The optimized parameters of the DPPTVI ions are listed in Table 1. As to the *solvent effect* on the geometric parameters, most of the changes in the bond lengths remain below 0.1 Å, the changes in the valence angles are all below 1°, the greater part of the torsion angles (τ) also change within 1°. Greater changes are observable in the environments of the nitro-

Table 1
Geometric parameters of the DPPTVI cation.

Parameter[a]	Isolated	Solute	Parameter[a]	Isolated	Solute
r (1, 2)	1.395	1.400	τ (3, 1, 2, 4)	0.1	0.1
r (1, 3)	1.395	1.399	τ (3, 1, 2,59)	−179.0	−179.3
r (1,60)	1.085	1.089	τ (60, 1, 2, 4)	179.8	179.9
r (2, 4)	1.387	1.392	τ (60, 1, 2,59)	0.7	0.5
r (2,59)	1.085	1.087	τ (2, 1, 3, 5)	0.2	0.2
r (3, 5)	1.397	1.402	τ (2, 1, 3,58)	179.9	179.9
r (3,58)	1.085	1.088	τ (60, 1, 3, 5)	−179.5	−179.6
r (4, 6)	1.393	1.396	τ (60, 1, 3,58)	0.2	0.2
r (4,10)	1.417	1.423	τ (1, 2, 4, 6)	−0.7	−0.6
r (5, 6)	1.385	1.389	τ (1, 2, 4,10)	179.4	179.5
r (5,57)	1.086	1.089	τ (59, 2, 4, 6)	178.5	178.8
r (6, 7)	1.508	1.515	τ (59, 2, 4,10)	−1.5	−1.2
r (7, 8)	1.541	1.549	τ (1, 3, 5, 6)	−0.1	0.0
r (7, 9)	1.538	1.546	τ (1, 3, 5,57)	179.8	179.8
r (7,12)	1.526	1.535	τ (58, 3, 5, 6)	−179.8	−179.7
r (8,54)	1.094	1.095	τ (58, 3, 5,57)	0.1	0.1
r (8,55)	1.095	1.095	τ (2, 4, 6, 5)	0.8	0.8
r (8,56)	1.094	1.095	τ (2, 4, 6, 7)	−179.4	−179.5
r (9,51)	1.094	1.095	τ (10, 4, 6, 5)	−179.2	−179.3
r (9,52)	1.094	1.095	τ (10, 4, 6, 7)	0.6	0.5
r (9,53)	1.094	1.095	τ (2, 4,10,11)	−6.7	−6.4
r (10,11)	1.449	1.459	τ (2, 4,10,12)	177.6	177.6
r (10,12)	1.342	1.346	τ (6, 4,10,11)	173.3	173.6
r (11,48)	1.091	1.091	τ (6, 4,10,12)	−2.4	−2.4
r (11,49)	1.092	1.092	τ (3, 5, 6, 4)	−0.4	−0.5
r (11,50)	1.095	1.095	τ (3, 5, 6, 7)	179.8	179.9
r (12,13)	1.402	1.407	τ (57, 5, 6, 4)	179.7	179.7
r (13,14)	1.384	1.386	τ (57, 5, 6, 7)	0.0	0.1
r (13,47)	1.086	1.087	τ (4, 6, 7, 8)	−116.5	−116.3
r (14,15)	1.416	1.423	τ (4, 6, 7, 9)	119.3	119.6
r (14,46)	1.086	1.086	τ (4, 6, 7,12)	1.1	1.3
r (15,16)	1.418	1.421	τ (5, 6, 7, 8)	63.3	63.3
r (15,18)	1.418	1.421	τ (5, 6, 7, 9)	−60.9	−60.7
r (16,21)	1.371	1.376	τ (5, 6, 7,12)	−179.1	−179.0
r (16,45)	1.088	1.090	τ (6, 7, 8,54)	−63.5	−63.4
r (17,18)	1.369	1.374	τ (6, 7, 8,55)	177.5	177.5
r (17,19)	1.430	1.434	τ (6, 7, 8,56)	56.0	56.2
r (17,44)	1.082	1.083	τ (9, 7, 8,54)	61.3	61.4
r (18,43)	1.086	1.089	τ (9, 7, 8,55)	−57.6	−57.7
r (19,20)	1.354	1.363	τ (9, 7, 8,56)	−179.1	−179.0
r (19,21)	1.425	1.429	τ (12, 7, 8,54)	−175.7	−175.6
r (20,22)	1.464	1.473	τ (12, 7, 8,55)	65.4	65.3
r (20,23)	1.464	1.473	τ (12, 7, 8,56)	−56.2	−56.0
r (21,42)	1.082	1.083	τ (6, 7, 9,51)	−177.0	−177.4
r (22,24)	1.529	1.538	τ (6, 7, 9,52)	63.8	63.3
r (22,40)	1.091	1.091	τ (6, 7, 9,53)	−55.9	−56.4
r (22,41)	1.097	1.097	τ (8, 7, 9,51)	58.3	58.1
r (23,25)	1.529	1.537	τ (8, 7, 9,52)	−60.9	−61.2
r (23,38)	1.097	1.097	τ (8, 7, 9,53)	179.5	179.1
r (23,39)	1.094	1.094	τ (12, 7, 9,51)	−64.4	−64.8
r (24,27)	1.523	1.531	τ (12, 7, 9,52)	176.4	175.9
r (24,36)	1.097	1.099	τ (12, 7, 9,53)	56.8	56.2
r (24,37)	1.097	1.098	τ (6, 7,12,10)	−2.5	−2.8
r (25,26)	1.524	1.532	τ (6, 7,12,13)	177.8	177.7
r (25,34)	1.096	1.097	τ (8, 7,12,10)	115.7	115.5
r (25,35)	1.097	1.097	τ (8, 7,12,13)	−63.9	−64.1
r (26,31)	1.096	1.097	τ (9, 7,12,10)	−121.5	−121.7
r (26,32)	1.096	1.097	τ (9, 7,12,13)	58.9	58.7
r (26,33)	1.094	1.095	τ (4,10,11,48)	−23.6	−22.2
r (27,28)	1.094	1.096	τ (4,10,11,49)	−141.9	−140.7
r (27,29)	1.095	1.096	τ (4,10,11,50)	96.5	97.9
r (27,30)	1.096	1.097	τ (12,10,11,48)	151.3	153.2
φ (2, 1, 3)	121.2	121.2	τ (12,10,11,49)	33.1	34.7
φ (2, 1,60)	119.1	119.0	τ (12,10,11,50)	−88.6	−86.7
φ (3, 1,60)	119.7	119.8	τ (4,10,12, 7)	3.1	3.3
φ (1, 2, 4)	116.9	116.9	τ (4,10,12,13)	−177.3	−177.2
φ (1, 2,59)	120.5	120.3	τ (11,10,12, 7)	−172.3	−172.5
φ (4, 2,59)	122.6	122.7	τ (11,10,12,13)	7.3	7.0
φ (1, 3, 5)	120.7	120.7	τ (7,12,13,14)	−164.5	−164.6
φ (1, 3,58)	119.6	119.7	τ (7,12,13,47)	10.7	11.0
φ (5, 3,58)	119.6	119.6	τ (10,12,13,14)	15.9	15.9
φ (2, 4, 6)	122.8	122.7	τ (10,12,13,47)	−168.8	−168.5
φ (2, 4,10)	128.4	128.5	τ (12,13,14,15)	179.4	179.6
φ (6, 4,10)	108.8	108.9	τ (12,13,14,46)	2.4	2.5
φ (3, 5, 6)	118.7	118.6	τ (47,13,14,15)	4.4	4.2
φ (3, 5,57)	120.3	120.4	τ (47,13,14,46)	−172.6	−172.8

Table 1 (*Continued*)

Parameter[a]	Isolated	Solute	Parameter[a]	Isolated	Solute
φ (6, 5,57)	121.1	121.0	τ (13,14,15,16)	−175.9	−176.8
φ (4, 6, 5)	119.7	119.9	τ (13,14,15,18)	4.1	3.5
φ (4, 6, 7)	109.0	109.0	τ (46,14,15,16)	1.2	0.3
φ (5, 6, 7)	131.3	131.1	τ (46,14,15,18)	−178.8	−179.4
φ (6, 7, 8)	111.4	111.3	τ (14,15,16,21)	−179.8	−179.7
φ (6, 7, 9)	111.8	111.8	τ (14,15,16,45)	0.9	0.7
φ (6, 7,12)	101.7	101.6	τ (18,15,16,21)	0.1	0.0
φ (8, 7, 9)	110.5	110.4	τ (18,15,16,45)	−179.2	−179.6
φ (8, 7,12)	110.4	110.5	τ (14,15,18,17)	−179.9	179.9
φ (9, 7,12)	110.8	110.9	τ (14,15,18,43)	0.8	0.4
φ (7, 8,54)	109.3	109.2	τ (16,15,18,17)	0.2	0.2
φ (7, 8,55)	111.2	111.1	τ (16,15,18,43)	−179.1	−179.3
φ (7, 8,56)	111.6	111.3	τ (15,16,21,19)	0.1	0.1
φ (54, 8,55)	107.8	108.1	τ (15,16,21,42)	−178.2	−179.1
φ (54, 8,56)	108.1	108.3	τ (45,16,21,19)	179.4	179.7
φ (55, 8,56)	108.7	108.7	τ (45,16,21,42)	1.1	0.6
φ (7, 9,51)	111.1	110.9	τ (19,17,18,15)	−0.7	−0.6
φ (7, 9,52)	109.5	109.4	τ (19,17,18,43)	178.6	179.0
φ (7, 9,53)	111.5	111.3	τ (44,17,18,15)	−179.6	−179.6
φ (51, 9,52)	108.0	108.2	τ (44,17,18,43)	−0.3	0.0
φ (51, 9,53)	108.5	108.6	τ (18,17,19,20)	−178.7	−179.1
φ (52, 9,53)	108.2	108.3	τ (18,17,19,21)	1.0	0.6
φ (4,10,11)	121.9	121.9	τ (44,17,19,20)	0.2	−0.1
φ (4,10,12)	111.2	111.2	τ (44,17,19,21)	179.8	179.6
φ (11,10,12)	126.7	126.8	τ (17,19,20,22)	171.3	171.6
φ (10,11,48)	108.7	108.7	τ (17,19,20,23)	−6.7	−5.2
φ (10,11,49)	109.4	109.4	τ (21,19,20,22)	−8.3	−8.1
φ (10,11,50)	111.5	111.2	τ (21,19,20,23)	173.8	175.1
φ (48,11,49)	108.5	108.7	τ (17,19,21,16)	−0.6	−0.4
φ (48,11,50)	108.9	109.1	τ (17,19,21,42)	177.6	178.7
φ (49,11,50)	109.8	109.7	τ (20,19,21,16)	178.9	179.3
φ (7,12,10)	109.2	109.2	τ (20,19,21,42)	−2.8	−1.6
φ (7,12,13)	121.8	121.8	τ (19,20,22,24)	106.8	107.3
φ (10,12,13)	128.9	129.0	τ (19,20,22,40)	−17.9	−17.3
φ (12,13,14)	128.9	128.6	τ (19,20,22,41)	−131.9	−131.8
φ (12,13,47)	113.2	113.6	τ (23,20,22,24)	−75.2	−75.7
φ (14,13,47)	117.6	117.7	τ (23,20,22,40)	160.2	159.7
φ (13,14,15)	126.9	126.8	τ (23,20,22,41)	46.2	45.2
φ (13,14,46)	118.6	119.0	τ (19,20,23,25)	−74.2	−76.2
φ (15,14,46)	114.4	114.1	τ (19,20,23,38)	50.6	48.3
φ (14,15,16)	119.3	119.1	τ (19,20,23,39)	164.8	162.9
φ (14,15,18)	124.4	124.5	τ (22,20,23,25)	107.7	106.8
φ (16,15,18)	116.4	116.5	τ (22,20,23,38)	−127.5	−128.7
φ (15,16,21)	122.5	122.4	τ (22,20,23,39)	−13.3	−14.2
φ (15,16,45)	118.8	118.8	τ (20,22,24,27)	−63.9	−63.7
φ (21,16,45)	118.7	118.8	τ (20,22,24,36)	173.9	174.5
φ (18,17,19)	121.6	121.6	τ (20,22,24,37)	59.9	60.3
φ (18,17,44)	118.4	117.9	τ (40,22,24,27)	59.9	60.4
φ (19,17,44)	120.0	120.4	τ (40,22,24,36)	−62.2	−61.5
φ (15,18,17)	121.9	121.8	τ (40,22,24,37)	−176.3	−175.7
φ (15,18,43)	120.0	120.2	τ (41,22,24,27)	176.2	176.6
φ (17,18,43)	118.1	118.0	τ (41,22,24,36)	54.1	54.8
φ (17,19,20)	120.9	121.0	τ (41,22,24,37)	−59.9	−59.4
φ (17,19,21)	116.6	116.5	τ (20,23,25,26)	179.3	−179.5
φ (20,19,21)	122.5	122.5	τ (20,23,25,34)	−58.8	−57.9
φ (19,20,22)	123.3	123.2	τ (20,23,25,35)	57.1	58.5
φ (19,20,23)	121.1	121.3	τ (38,23,25,26)	55.1	56.4
φ (22,20,23)	115.6	115.5	τ (38,23,25,34)	176.9	178.0
φ (16,21,19)	121.0	121.1	τ (38,23,25,35)	−67.2	−65.6
φ (16,21,42)	118.5	118.1	τ (39,23,25,26)	−61.0	−59.9
φ (19,21,42)	120.4	120.8	τ (39,23,25,34)	60.8	61.7
φ (20,22,24)	114.6	114.9	τ (39,23,25,35)	176.7	178.1
φ (20,22,40)	109.1	109.3	τ (22,24,27,28)	178.4	179.2
φ (20,22,41)	106.7	106.8	τ (22,24,27,29)	58.5	59.4
φ (24,22,40)	110.6	110.3	τ (22,24,27,30)	−62.2	−61.1
φ (24,22,41)	109.5	109.0	τ (36,24,27,28)	−61.2	−60.6
φ (40,22,41)	105.9	106.2	τ (36,24,27,29)	179.0	179.6
φ (20,23,25)	114.4	114.6	τ (36,24,27,30)	58.3	59.1
φ (20,23,38)	109.5	109.5	τ (37,24,27,28)	55.0	55.6
φ (20,23,39)	106.8	106.7	τ (37,24,27,29)	−64.8	−64.2
φ (25,23,38)	110.6	110.3	τ (37,24,27,30)	174.4	175.2
φ (25,23,39)	109.3	109.2	τ (23,25,26,31)	59.8	59.8
φ (38,23,39)	105.9	106.2	τ (23,25,26,32)	−60.5	−60.4
φ (22,24,27)	114.4	114.8	τ (23,25,26,33)	179.6	179.7
φ (22,24,36)	107.0	106.7	τ (34,25,26,31)	−61.3	−61.3
φ (22,24,37)	109.2	109.3	τ (34,25,26,32)	178.4	178.5
φ (27,24,36)	110.0	109.8	τ (34,25,26,33)	58.5	58.6

Table 1 (*Continued*)

Parameter[a]	Isolated	Solute	Parameter[a]	Isolated	Solute
φ (27,24,37)	110.0	109.9	τ (35,25,26,31)	−178.1	−178.2
φ (36,24,37)	105.8	106.0	τ (35,25,26,32)	61.6	61.7
φ (23,25,26)	111.5	111.5	τ (35,25,26,33)	−58.3	−58.2
φ (23,25,34)	109.0	109.1			
φ (23,25,35)	109.8	109.9			
φ (26,25,34)	110.2	109.9			
φ (26,25,35)	110.1	109.8			
φ (34,25,35)	106.2	106.5			
φ (25,26,31)	111.4	111.3			
φ (25,26,32)	111.5	111.3			
φ (25,26,33)	110.9	110.9			
φ (31,26,32)	107.6	107.7			
φ (31,26,33)	107.6	107.8			
φ (32,26,33)	107.6	107.7			
φ (24,27,28)	110.7	110.6			
φ (24,27,29)	111.6	111.5			
φ (24,27,30)	111.5	111.4			
φ (28,27,29)	107.6	107.7			
φ (28,27,30)	107.3	107.6			
φ (29,27,30)	107.9	107.8			

[a] *r*: bond lengths, in angstroms; φ: valence angles in degrees; τ: torsional angles in degrees.

gen atoms. The N10–C12 bond is increased by +0.1 Å or a little more. The C4–N10–C11–H48, the C4–N10–C11–H49 and the C4–N10–C11–H50 torsion angles increased more than 1°, in contrast to other torsion angles of this NCH_3 group describing the torsion to the C11–N10 bond, decreasing 0.1 Å or a bit more. The situation is similar around N20. The solvent effects of the N20–C19, N20–C22 and N20–C23 bonds are +0.09 Å. The C21–C19–N20–C23, C19–N20–C23–C25 and C22–N20–C23–H38 torsion angles show positive (1.0–2.5°, absolute value) solvent effects, while the C17–C19–N20–C23, the N20–C19–C21–H42, the C19–N20–C23–H38 and the C19–N20–C23–H39 torsion angles show negative solvent effects to a similar measure.

Especially interesting is the C4–N10–C12–C13–C14–C15 chain. The corresponding bond lengths are 1.417, 1.346, 1.402, 1.384 and 1.416 Å, respectively. According to [27] the single C–C bond length is about 1.54 Å, that of C=C one is 1.34 Å, the single N–C bond length is 1.42 Å, while the N=C double bond length is expected according to [28], to be 1.317 Å. That means, the C4–N10 bond is a real C–N one, the N10–C12 bond length is between those for the single and the double bond lengths, the C12–C13 bond is similarly partly double bond, the C13–C14 bond length is like the one for an aromatic CC bond (see Table 1, e.g. C1–C2 or C5–C6), while the C14–C15 bond is again partly double bond. The N10 atom has an effect on the benzene ring of the indole; the bonds closer to this atom are shorter than the others in the ring. All these facts support the existence of an extended conjugation between the two aromatic rings.

4.2. Atomic charges

Both Mulliken's atomic net charges [29] and the natural NBO/NPA atomic charges [30,31] were calculated. The results are listed in Table 2.

The comparison between Mulliken's net charges and the atomic natural ones is not an easy task since these two methods have quite different theoretical background. The results show remarkable differences between the Mulliken's and the NBO charges.

The definition of Mulliken's charges is based on population analysis. The *Mulliken population analysis* provides a partitioning of either the total charge density or an orbital density. The number of the electrons in the molecule (*N*) is the integral of the charge density over the space. *N* is partitioned for all atoms, the overlap population is also considered. According to the theory, the overlap population of atoms A and B is divided between the two atoms in half-to-half ratio. This is one weak point of the theory. The other weak point is its strong dependence on the applied basis set. Our Mulliken's atomic net charges are comparable since the same basis set was used for both the isolated and the solute compounds. The atomic net charge is the difference between the calculated number of electrons belonging to the atom in the molecule and the number of electrons of the isolated atom.

The natural atomic charge is based on the theory of *natural population analysis*. The analysis is carried out with natural bond orbitals (NBO). They are linear combinations of the natural atomic orbitals. The derivation of a valence-shell atomic orbital (NAO) involves diagonalization of the localized block of the full density matrix of a given molecule associated with basis functions on the atom. A distinguishing feature of NAOs is that they meet the simultaneous requirement of orthonormality and maximum occupancy. In a polyatomic molecule NAOs mostly retain one-center character, and thus they are optimal for describing the molecular electron density around each atomic center. Natural bond orbitals are linear combinations of NAOs of two bonded atoms. The natural population analysis satisfies Pauli's exclusion principle and solves the basis set dependence problem of the Mulliken's population analysis.

As seen from Table 2. we regarded *NBO charges* more important. All carbon atoms are around benzene ring rg1 have negative charges, however, C6 is the least negative one. An other carbon atom of the five membered ring C12, has a positive charge. Both are nearest neighbors of N10. The negative charges of the carbon atoms of the $N(C_3H_7)_2$ group increase radically with the increasing distance from the N20 atom, e.g. for C22 the charge is −0.273 atomic charge unit (a.ch.u.), for C26 it is −0.710 a.ch.u. The atom C19 of the rg2 ring in the vicinity of N20 has positive charge, as well. The strong electron repulsive inductive effects of the NR_3 groups in the positive ion are clearly observable. One can conclude, that N20 affects stronger on its vicinity than N10. The Mulliken net charge distributions show similar effects. However, the NBO charge of N10

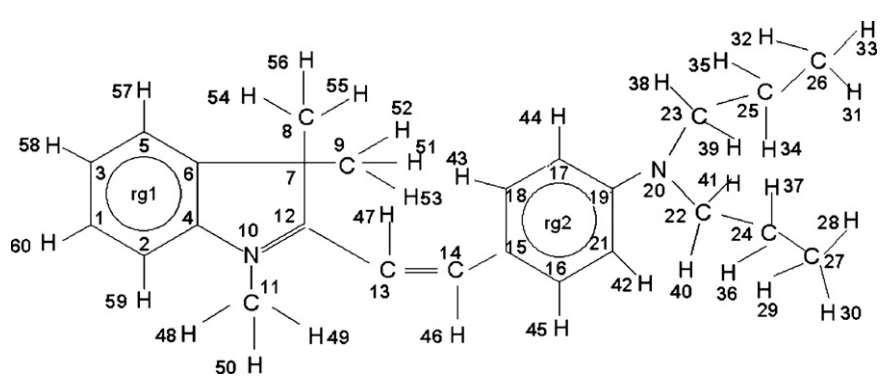

Fig. 2. Numbering of the DPPTVI atoms and rings.

Table 2
Atomic charges of the DPPTVI cation[a].

Serial number	Atom type	Mulliken net charges		NBO charges		number	Atom type	Mulliken net charges		NBO charges	
		Isolated	PCM	Isolated	PCM			Isolated	PCM	Isolated	PCM
1	C	−0.172	−0.164	−0.217	−0.226	31	H	0.183	0.153	0.244	0.230
2	C	−0.193	−0.193	−0.261	−0.259	32	H	0.175	0.153	0.239	0.230
3	C	−0.160	−0.154	−0.225	−0.237	33	H	0.195	0.156	0.259	0.241
4	C	0.330	0.325	0.152	0.157	34	H	0.186	0.158	0.249	0.237
5	C	−0.226	−0.230	−0.215	−0.219	35	H	0.178	0.156	0.245	0.238
6	C	0.101	0.111	−0.040	−0.040	36	H	0.191	0.157	0.263	0.249
7	C	−0.147	−0.097	−0.103	−0.094	37	H	0.178	0.156	0.244	0.235
8	C	−0.500	−0.455	−0.683	−0.661	38	H	0.194	0.178	0.247	0.243
9	C	−0.496	−0.451	−0.684	−0.662	39	H	0.197	0.179	0.258	0.251
10	N	−0.589	−0.560	−0.332	−0.331	40	H	0.194	0.182	0.248	0.245
11	C	−0.420	−0.367	−0.504	−0.483	41	H	0.202	0.179	0.259	0.251
12	C	0.417	0.409	0.343	0.349	42	H	0.189	0.181	0.256	0.256
13	C	−0.210	−0.208	−0.350	−0.344	43	H	0.183	0.189	0.249	0.258
14	C	−0.188	−0.173	−0.104	−0.091	44	H	0.189	0.179	0.257	0.257
15	C	0.144	0.148	−0.144	−0.148	45	H	0.184	0.187	0.252	0.261
16	C	−0.215	−0.211	−0.161	−0.162	46	H	0.182	0.182	0.239	0.243
17	C	−0.208	−0.203	−0.285	−0.289	47	H	0.178	0.180	0.253	0.256
18	C	−0.197	−0.201	−0.165	−0.166	48	H	0.227	0.210	0.265	0.259
19	C	0.391	0.383	0.242	0.237	49	H	0.224	0.208	0.262	0.257
20	N	−0.480	−0.476	−0.380	−0.392	50	H	0.226	0.215	0.258	0.256
21	C	−0.204	−0.206	−0.289	−0.294	51	H	0.184	0.169	0.250	0.245
22	C	−0.225	−0.178	−0.273	−0.259	52	H	0.199	0.175	0.261	0.250
23	C	−0.213	−0.168	−0.285	−0.269	53	H	0.199	0.172	0.261	0.249
24	C	−0.317	−0.264	−0.493	−0.472	54	H	0.202	0.177	0.263	0.252
25	C	−0.323	−0.268	−0.488	−0.468	55	H	0.184	0.172	0.248	0.244
26	C	−0.520	−0.456	−0.710	−0.682	56	H	0.200	0.173	0.261	0.249
27	C	−0.521	−0.457	−0.713	−0.686	57	H	0.188	0.181	0.259	0.263
28	H	0.196	0.154	0.259	0.240	58	H	0.197	0.174	0.264	0.260
29	H	0.177	0.155	0.239	0.230	59	H	0.192	0.192	0.258	0.266
30	H	0.171	0.152	0.236	0.228	60	H	0.199	0.178	0.265	0.262

[a] Atomic charge units.

(−0.332 a.ch.u.) is less negative than N20 (−0.380 a.ch.u.), while in case of the corresponding Mulliken charges the order is opposite.

Comparison of the NBO charges of the isolated and aqueous solute ions show positive changes in the N10 environment, e.g. the C9 charge increases by 0.018 a.ch.u., C21 by 0.021 a.ch.u. The N10 charge remains practically unchanged. All carbon charges in the $N(C_3H_7)_2$ group exhibit positive changes between 0.014 and 0.027 a.ch.u. The carbon atoms of the vinylydene group became more positive but remain negatively charged, although this negative charge is reduced (C13 and C14). One cannot characterize unambiguously the changes in other carbon atom charges and the hydrogen atom charges.

For the Mulliken charges the character of the charge variation shows similar tendencies but the changes are greater. The calculated *dipole moment* of the isolated ion is 1.905 D, while that of the solute ion increases to 2.874 D.

The *energy* of the isolated ion decreases in the aqueous solution by 9.191 kJ/mol.

4.3. Vibrational force constants

The vibrational force constants provide information about the interatomic forces in the molecule. However, it is a challenge to extract this information since the molecules in question with their 60 atoms have 174 vibrational modes and accordingly the force constant matrices have 174 × 174 elements. Of course, the full force constant matrix was applied in the GF matrix eigenvector–eigenvalue calculations. For practical use, only the diagonal elements are presented (see Table 3).

As mentioned above, the values of the applied 12 scale factors remained between 0.877 and 0.921 (Table 3).

Here we also have to deal with the problem of the definition of the internal coordinates. The molecules contain two phenolic rings. The first problem is the indolene ring. One can define the coordinates of the benzene ring according to the intentions of Fogarasi and coworkers [32]. One can follow them also for the full indolene skeleton. However, in this case the value of the G matrix determinant radically decreases. Following the definitions of the internal coordinates one find the problem of the second benzene ring. Here one can define only 12 coordinates (3 × 6–6) but 18 ones are necessary. Six new coordinates should be added. We tried to define them in several forms, however, only one simple form gave non-zero G matrix determinant (coordinates 91–108), if the coordinates of the pyrrolidine ring coordinates (coordinates 25–33) were also defined in the similar simple way. We have to note that if the coordinates were defined in a different way, the G matrix determinant of the skeleton was zero. The problem of the choice of coordinates

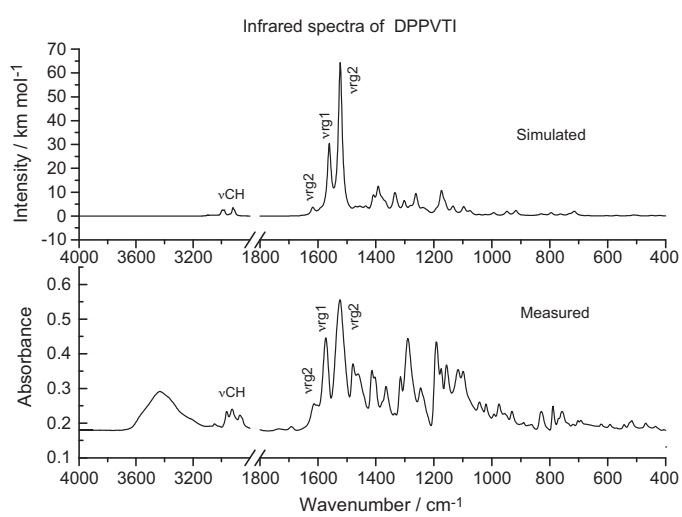

Fig. 3. Infrared spectra of the DPPVTI compound and its simulation for the isolated cation.

Table 3
Diagonal force constants of the DPPTVI cation.

Internal coordinate		Scale factor	Diagonal force constant[b]		Internal coordinate		Scale factor	Diagonal force constant[b]	
Ser. no.	Definition[a]		Isolated	Solute	Ser. no.	Definition[a]		Isolated	Solute
1	r (2,1)	0.877	12.211	11.803	75	ϑ (47,12,14,13)	0.908	0.388	0.398
2	r (1,3)	0.877	7.017	6.816	76	r (14,13)	0.905	6.747	6.541
3	r (3,5)	0.877	7.444	7.210	77	φ (14,12,13)	0.921	1.652	1.658
4	r (5,6)	0.877	7.114	6.919	78	τ (14,13,12,10)	0.898	0.304	0.283
5	r (6,4)	0.877	15.321	14.794	79	r (46,14)	0.901	5.129	5.109
6	r (4,1)	0.877	14.376	13.913	80	φ (46,13,14)	0.904	1.090	1.116
7	φ (2,3,1)	0.906	4.325	4.283	81	ϑ (46,15,13,14)	0.908	0.443	0.443
	$-\varphi$ (4,1,2)				82	r (15,14)	0.905	6.032	5.718
	$+\varphi$ (6,2,4)				83	φ (15,13,14)	0.921	1.614	1.652
	$-\varphi$ (5,4,6)				84	τ (15,14,13,12)	0.898	0.295	0.286
	$+\varphi$ (3,6,5)				85	r (16,15)	0.905	7.991	7.726
	$-\varphi$ (1,5,3)				86	φ (16,14,15)	0.921	15.977	15.663
8	2φ (2,3,1)	0.906	3.833	3.794	87	τ (16,15,14,13)	0.898	0.286	0.281
	$-\varphi$ (4,1,2)				88	r (45,16)	0.901	5.071	4.871
	$-\varphi$ (6,2,4)				89	φ (45,15,16)	0.904	1.017	1.023
	$+2\varphi$ (5,4,6)				90	ϑ (45,15,21,16)	0.908	0.427	0.435
	$-\varphi$ (3,6,5)				91	r (18,15)	0.905	8.761	8.528
	$-\varphi$ (1,5,3)				92	φ (18,14,15)	0.921	15.887	15.601
9	φ (1,5,3)	0.906	5.786	5.722	93	τ (18,15,14,13)	0.898	0.321	0.320
	$-\varphi$ (3,6,5)				94	r (43,18)	0.901	5.128	4.929
	$+\varphi$ (6,2,4)				95	φ (43,15,18)	0.904	1.012	1.036
	$-\varphi$ (4,1,2)				96	ϑ (43,17,15,18)	0.908	0.405	0.414
10	τ (5,3,1,2)	0.871	0.573	0.578	97	r (17,18)	0.905	15.135	14.530
	$-\tau$ (3,1,2,4)				98	φ (17,15,18)	0.921	45.924	44.491
	$+\tau$ (1,2,4,6)				99	τ (17,18,15,16)	0.898	3.904	3.864
	$-\tau$ (2,4,6,5)				100	r (44,17)	0.901	5.252	5.126
	$+\tau$ (4,6,5,3)				101	φ (44,18,17)	0.904	1.035	1.052
	$-\tau$ (6,5,3,1)				102	ϑ (44,18,19,17)	0.908	0.390	0.390
11	τ (5,3,1,2)	0.871	2.410	2.438	103	r (19,17)	0.905	8.451	8.226
	-2τ (3,1,2,4)				104	φ (19,18,17)	0.921	46.383	44.955
	$+\tau$ (1,2,4,6)				105	τ (19,17,18,15)	0.898	7.524	7.498
	$+\tau$ (2,4,6,5)				106	r (21,19)	0.905	7.535	7.268
	-2τ (4,6,5,3)				107	φ (21,17,19)	0.921	16.839	16.617
	$+\tau$ (6,7,3,1)				108	τ (21,19,17,18)	0.898	4.312	4.347
12	τ (5,3,1,2)	0.871	1.138	1.146	109	r (42,21)	0.901	5.267	5.129
	$-\tau$ (3,1,2,4)				110	φ (42,19,21)	0.904	1.030	1.048
	$+\tau$ (2,4,6,5)				111	ϑ (42,16,19,21)	0.908	0.382	0.389
	$-\tau$ (4,6,5,3)				112	r (20,19)	0.925	7.387	6.871
13	r (57,5)	0.901	5.116	4.903	113	φ (20,21,19)	0.902	3.095	3.140
14	φ (57,3,5)	0.904	0.959	0.969	114	τ (20,19,21,16)	0.897	0.545	0.532
15	ϑ (57,3,6,5)	0.908	0.424	0.427	115	r (22,20)	0.925	4.648	4.429
16	r (58,3)	0.901	5.161	4.941	116	φ (22,19,20)	0.902	2.601	2.652
17	φ (58,1,3)	0.904	0.987	0.975	117	τ (22,20,19,17)	0.897	0.328	0.342
18	ϑ (58,1,5,3)	0.908	0.428	0.423	118	r (24,22)	0.905	3.983	3.809
19	r (60,1)	0.901	5.159	4.939	119	φ (24,20,22)	0.921	1.447	1.453
20	φ (60,2,1)	0.904	0.989	0.978	120	τ (24,22,20,19)	0.898	0.978	0.983
21	ϑ (60,2,3,1)	0.908	0.432	0.429	121	r (27,24)	0.905	4.193	4.012
22	r (59,2)	0.901	5.160	4.973	122	φ (27,22,24)	0.921	1.341	1.331
23	φ (59,1,2)	0.904	0.963	0.983	123	τ (27,24,22,20)	0.898	0.868	0.867
24	ϑ (59,4,1,2)	0.908	0.386	0.389	124	r (41,22)	0.901	4.722	4.645
25	r (7,6)	0.905	10.329	9.926	125	φ (41,20,22)	0.904	1.083	1.089
26	φ (7,4,6)	0.921	39.232	38.146	126	τ (41,22,20,19)	0.908	0.814	0.815
27	τ (7,6,5,3)	0.898	1.193	1.206	127	r (40,22)	0.901	4.939	4.885
28	r (12,7)	0.905	5.451	5.261	128	φ (40,20,22)	0.904	1.061	1.078
29	φ (12,6,7)	0.921	22.581	22.226	129	τ (40,22,20,19)	0.908	0.767	0.772
30	τ (12,7,6,5)	0.898	5.165	5.262	130	r (36,24)	0.901	4.741	4.635
31	r (10,4)	0.925	7.080	6.842	131	φ (36,22,24)	0.904	0.929	0.929
32	φ (10,2,4)	0.902	17.969	17.706	132	τ (36,24,22,20)	0.908	0.811	0.813
33	τ (10,4,2,1)	0.897	2.130	2.154	133	r (37,24)	0.901	4.726	4.655
34	r (8,7)	0.905	3.824	3.658	134	φ (37,22,24)	0.904	0.967	0.969
35	φ (8,6,7)	0.921	1.402	1.459	135	τ (37,24,22,20)	0.908	0.793	0.796
36	τ (8,7,6,4)	0.898	1.130	1.154	136	r (28,27)	0.901	4.873	4.765
37	r (55,8)	0.901	4.849	4.791	137	φ (28,24,27)	0.904	0.883	0.880
38	φ (55,7,8)	0.904	0.890	0.903	138	τ (28,27,24,22)	0.908	0.706	0.708
39	τ (55,8,7,6)	0.908	0.696	0.706	139	r (30,27)	0.901	4.798	4.734
40	r (54,8)	0.901	4.874	4.797	140	φ (30,24,27)	0.904	0.893	0.896
41	φ (54,7,8)	0.904	0.894	0.899	141	τ (30,27,24,22)	0.908	0.706	0.713
42	τ (54,8,7,6)	0.908	0.708	0.715	142	r (29,27)	0.901	4.824	4.766
43	r (56,8)	0.901	4.889	4.808	143	φ (29,24,27)	0.904	0.904	0.900
44	φ (56,7,8)	0.904	0.900	0.904	144	τ (29,27,24,22)	0.908	0.707	0.713
45	τ (56,8,7,6)	0.908	0.693	0.699	145	r (23,20)	0.925	4.667	4.456
46	r (9,7)	0.905	3.883	3.717	146	φ (23,19,20)	0.902	2.492	2.540
47	φ (9,12,7)	0.921	1.363	1.400	147	τ (23,20,19,17)	0.897	0.409	0.391
48	τ (9,7,12,10)	0.898	1.165	1.199	148	r (25,23)	0.905	3.971	3.804

Table 3 (*Continued*)

Internal coordinate		Scale factor	Diagonal force constant[b]		Internal coordinate		Scale factor	Diagonal force constant[b]	
Ser. no.	Definition[a]		Isolated	Solute	Ser. no.	Definition[a]		Isolated	Solute
49	r (53,9)	0.901	4.891	4.808	149	φ (25,20,23)	0.921	1.322	1.330
50	φ (53,7,9)	0.904	0.902	0.905	150	τ (25,23,20,19)	0.898	1.090	1.064
51	τ (53,9,7,12)	0.908	0.692	0.699	151	r (26,25)	0.905	4.184	4.007
52	r (51,9)	0.901	4.860	4.800	152	φ (26,23,25)	0.921	1.200	1.209
53	φ (51,7,9)	0.904	0.893	0.903	153	τ (26,25,23,20)	0.898	0.841	0.852
54	τ (51,9,7,12)	0.908	0.692	0.703	154	r (39,23)	0.901	4.837	4.754
55	r (52,9)	0.901	4.872	4.797	155	φ (39,20,23)	0.904	1.105	1.120
56	φ (52,7,9)	0.904	0.884	0.892	156	τ (39,23,20,19)	0.908	0.807	0.811
57	τ (52,9,7,12)	0.908	0.704	0.712	157	r (38,23)	0.901	4.694	4.641
58	r (11,10)	0.925	4.969	4.689	158	φ (38,20,23)	0.904	1.038	1.052
59	φ (11,4,10)	0.902	2.069	2.130	159	τ (38,23,20,19)	0.908	0.805	0.809
60	τ (11,10,4,6)	0.897	0.225	0.223	160	r (34,25)	0.901	4.768	4.699
61	r (49,11)	0.901	4.931	4.878	161	φ (34,23,25)	0.904	0.948	0.950
62	φ (49.10.11)	0.904	0.984	0.988	162	τ (34,25,23,20)	0.908	0.789	0.791
63	τ (49.11.10.4)	0.908	0.741	0.742	163	r (35,25)	0.901	4.749	4.693
64	r (50,11)	0.901	4.820	4.771	164	φ (35,23,25)	0.904	0.951	0.955
65	φ (50.10.11)	0.904	0.968	0.970	165	τ (35,25,23,20)	0.908	0.787	0.789
66	τ (50.11.10.4)	0.908	0.704	0.710	166	r (31,26)	0.901	4.814	4.726
67	r (48,11)	0.901	4.995	4.950	167	φ (31,25,26)	0.904	0.906	0.900
68	φ (48,10,11)	0.904	1.016	1.030	168	τ (31,26,25,23)	0.908	0.703	0.708
69	τ (48,11,10,4)	0.908	0.718	0.715	169	r (33,26)	0.901	4.885	4.780
70	r (13,12)	0.905	6.269	5.997	170	φ (33,25,26)	0.904	0.877	0.874
71	φ (13,7,12)	0.921	2.519	2.557	171	τ (33,26,25,23)	0.908	0.698	0.701
72	τ (13,12,7,6)	0.898	0.705	0.685	172	r (32,26)	0.901	4.794	4.722
73	r (47,13)	0.901	5.113	5.042	173	φ (32,25,26)	0.904	0.902	0.900
74	φ (47,12,13)	0.904	1.090	1.126	174	τ (32,26,25,23)	0.908	0.697	0.705

[a] r: stretching; φ: in-plane deformation; τ: torsion; ϑ: o.o.p. deformation; for the position of the atoms see Fig. 2.
[b] Units: for stretching coordinates 10^2 N m^{-1}, for deformation coordinates 10^{-18} N m.

resulted in the values of the diagonal elements of the deformation force constants of the mentioned critical parts of the molecules. These extremely high values reflect the tension generated by the performed definition of the internal coordinates. Consequently, at this choice of coordinates some of them are nonlinear. However, here they were regarded as being linear ones. The solvent slightly moderated these extreme values (see Table 3 for the definition of the internal coordinates).

4.4. Characterization of the vibrational modes

The measured and calculated vibrational frequencies of the isolated DPPTVI ion are listed in Table 4 . The potential energy distributions of several chemically similar internal coordinates are summarized. That means, the weights of all CH stretchings (νCH), in-plane deformations (βCH) and out-of-plane deformations (γCH) are grouped for each vibrational mode, respectively. The skeleton vibrations are similarly grouped, the internal coordinates belonging to the benzene ring of the indolene part, are presented as rg1 (torsions are labeled as τ), the internal coordinates of the other benzene ring as rg2. The cation contains two nitrogen atoms, N10 and N20. The coordinates including N10 are summarized under CN1, those with N20 are found under CN2.

Only CH vibrations can be regarded as characteristic ones, first of all the CH stretchings, some in-plane and out-of-plane deformations. Besides, some CC torsion modes exist. In the

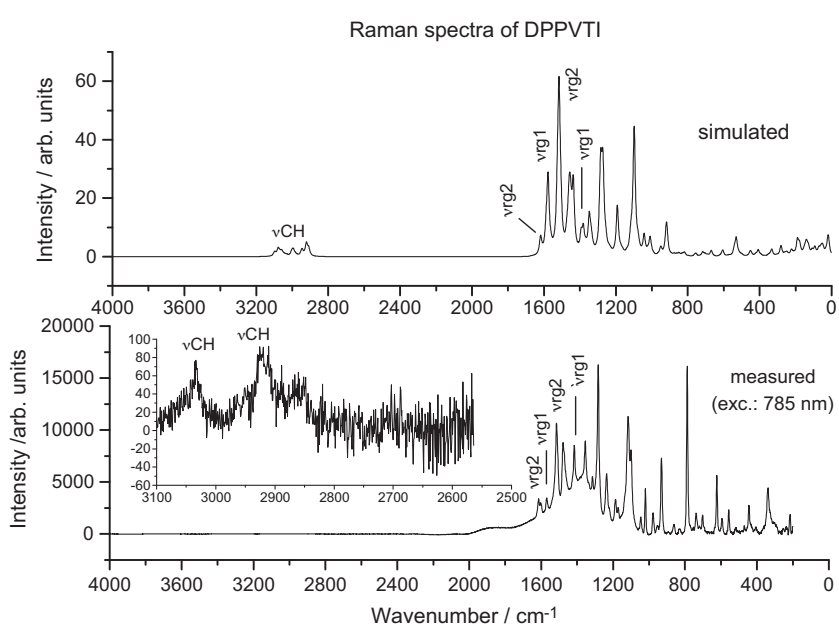

Fig. 4. Raman spectra of the DPPVTI compound and its simulation for the isolated cation.

Table 4
Properties of vibrational modes of the isolated DPPTVI cation.

Frequency (cm^{-1})		Potential energy distribution[a] (%)														
Measured	Calculated															
3097.6	3099.0	ν	CH	98												
3097.6	3094.8	ν	CH	99												
3078.4	3077.6	ν	CH	99												
3078.4	3068.8	ν	CH	99												
3051.9	3059.8	ν	CH	99												
3051.9	3057.9	ν	CH	99												
3051.9	3054.9	ν	CH	99												
3051.9	3050.7	ν	CH	99												
3041.1	3043.7	ν	CH	99												
3041.1	3039.1	ν	CH	99												
3020.3	3029.7	ν	CH	99												
3020.3	3003.3	ν	CH	99												
3012.8	3002.5	ν	CH	99												
3012.8	3001.9	ν	CH	99												
3012.8	2999.1	ν	CH	91												
2983.7	2996.3	ν	CH	99												
2983.5	2993.9	ν	CH	99												
2983.5	2992.9	ν	CH	99												
2983.5	2990.7	ν	CH	99												
2983.5	2981.4	ν	CH	99												
2963.4	2979.1	ν	CH	99												
2963.4	2970.9	ν	CH	99												
2963.4	2948.4	ν	CH	99												
2963.4	2943.8	ν	CH	97												
2926.7	2923.5	ν	CH	99												
2926.7	2921.5	ν	CH	99												
2926.7	2919.3	ν	CH	97												
2926.7	2918.7	ν	CH	99												
2926.7	2916.6	ν	CH	99												
2890.8	2910.5	ν	CH	96												
2890.8	2908.4	ν	CH	99												
2890.8	2907.1	ν	CH	93												
2890.8	2906.3	ν	CH	98												
1614.7	1618.2	ν	rg2	52	ν	CC	13	β	CH	18						
1601.3	1586.8	ν	rg1	57	β	rg1	10	β	CH	13						
1573.4	1575.6	ν	rg1	54	β	CC	17	β	CH	13						
1568.8	1560.5	ν	rg1	10	ν	rg2	13	ν	CC	34	β	CH	30			
1524.0	1522.7	ν	rg2	13	ν	CN2	13	ν	CC	26	β	CH	25			
1514.4	1514.6	ν	rg2	13	β	CN1	14	ν	CN2	16	ν	CC	10	β	CC	15
1514.4	1506.3	ν	rg2	49	β	rg2	19	β	CH	14						
1479.5	1472.9	β	rg2	12	β	CH	15	β	CH	22	γ	CH	35			
1473.2	1470.4	β	rg2	20	β	CH	26	γ	CH	13	γ	CH	15			
1461.9	1461.3	β	CH	23	γ	CH	60									
1461.9	1458.4	β	CH	25	γ	CH	44									
1461.9	1456.2	β	CH	20	γ	CH	68									
1461.9	1454.4	β	CH	23	γ	CH	69									
1461.9	1453.7	β	CH	27	γ	CH	56									
1461.9	1452.8	β	CH	21	γ	CH	76									
1439.8	1451.1	β	CH	23	γ	CH	72									
1439.8	1448.1	β	CH	13	γ	CH	65									
1439.8	1446.5	β	CH	12	γ	CH	70									
1439.8	1445.0	β	CH	16	γ	CH	70									
1439.8	1438.7	β	CH	19	γ	CH	55									
1426.5	1435.5	ν	rg1	10	β	CH	66									
1426.5	1434.5	β	CH	17	γ	CH	81									
1426.5	1430.8	ν	rg1	13	β	CH	29	γ	CH	48						
1426.5	1430.4	ν	rg1	15	β	CH	31	γ	CH	44						
1415.6	1409.2	ν	CN2	11	β	CH	41									
1402.9	1392.2	β	CH	60												
1378.4	1379.5	β	CH	73												
1365.2	1373.5	β	CH	87												
1365.2	1370.2	β	CH	95												
1365.2	1366.5	β	CH	72												
1354.7	1350.2	β	CH	99												
1354.7	1347.4	β	CH	54	γ	CH	24									
1334.7	1337.9	ν	rg1	54	ν	CN1	13	β	CH	14						
1334.7	1333.8	β	CH	52	γ	CH	19									
1334.7	1331.0	ν	rg2	31	β	CH	29									
1315.4	1324.5	β	CH	69	γ	CH	10									
1289.5	1302.2	β	CH	71												
1289.5	1283.6	ν	rg1	10	ν	CN1	22	β	CH	28	β	CH	11			
1270.4	1278.9	β	CH	62	γ	CH	11									
1270.4	1271.4	β	CH	63	γ	CH	12									
1270.4	1270.0	β	CH	64	γ	CH	10									

Table 4 (*Continued*)

Frequency (cm^{-1})		Potential energy distribution[a] (%)														
Measured	Calculated															
1243.3	1261.8	ν	CC	33	β	CH	45									
1243.3	1254.6	β	CH	67	γ	CH	18									
1236.0	1238.8	β	CH	63	γ	CH	14									
1236.0	1231.0	ν	rg2	11	β	CH	64									
1219.8	1226.6	ν	CC	10	β	CH	52	γ	CH	12						
1219.8	1221.1	ν	CC	27	β	CH	36									
1191.4	1191.3	ν	rg1	15	ν	CC	27	β	CH	33						
1174.3	1173.7	ν	rg2	12	β	CH	63									
1174.3	1168.8	ν	CN2	23	β	CH	30	γ	CH	18						
1156.2	1160.8	ν	rg1	10	ν	CC	19	β	CH	26						
1132.8	1137.9	ν	rg1	18	β	CH	76									
1132.8	1132.8	τ	CC	12	β	CH	36	γ	CH	19						
1116.3	1118.0	β	rg2	35	β	CH	37									
1116.3	1112.5	ν	CC	50	β	CH	41									
1099.7	1098.8	ν	rg1	26	β	CH	49									
1096.7	1097.2	ν	rg1	28	β	CH	49									
1096.7	1090.5	β	CH	73	γ	CH	16									
1096.7	1083.9	ν	CC	25	β	CC	13	β	CH	42						
1096.7	1075.0	ν	CN2	17	ν	CC	16	β	CH	41						
1042.9	1067.2	ν	CC	34	β	CC	13	β	CH	36						
1042.9	1042.2	β	rg1	41	β	CH	25									
1019.7	1022.1	ν	CC	65	β	CH	16									
1019.7	1008.6	ν	rg1	12	ν	CN1	18	ν	CC	19	β	CH	26			
992.9	1004.3	ν	CC	62	β	CH	22									
992.9	993.4	ν	rg1	61	β	CH	19									
975.4	987.8	β	CH	74	γ	CH	17									
953.6	963.4	ν	rg2	54	β	rg2	23	β	CH	19						
953.6	956.0	γ	CH	84												
953.6	950.0	ν	CN2	10	γ	CH	57									
953.6	947.4	ν	CN2	16	β	CH	14	γ	CH	42						
929.8	921.9	γ	CH	57												
929.8	919.8	ν	CC	16	β	CH	34	γ	CH	40						
929.8	917.7	β	CH	15	γ	CH	59									
899.0	915.8	ν	CC	11	β	CH	11	γ	CH	53						
899.0	907.4	γ	CH	89												
890.2	890.1	ν	CC	28	β	CC	27	β	CH	16						
860.4	875.2	ν	CC	35	β	CH	36	γ	CH	12						
860.4	860.7	ν	CC	21	β	CH	36	γ	CH	23						
860.4	848.0	ν	CC	15	β	CH	32	γ	CH	25						
829.0	836.6	γ	CH	96												
829.0	831.0	γ	CH	84												
829.0	828.5	ν	CC	45	β	CH	12	γ	CH	28						
829.0	817.2	ν	rg2	34	β	rg2	16	ν	CC	21						
788.8	794.6	τ	rg2	11	γ	CH	81									
771.0	763.7	γ	CH	78												
757.3	762.7	β	CH	13	γ	CH	51									
757.3	755.1	β	rg1	28	ν	CN1	13	ν	CC	15	β	CC	12			
738.1	733.3	γ	CH	81												
719.6	719.9	τ	rg1	63	τ	CC	15									
719.6	717.5	β	CH	24	γ	CH	65									
719.6	713.5	β	rg2	11	ν	CN2	13	β	CC	14	γ	CH	11			
703.2	702.4	τ	rg2	73												
692.7	689.0	ν	rg1	12	β	rg1	19	β	rg2	10	ν	CC	18	β	CC	10
678.4	668.3	τ	rg1	18	τ	rg2	14	τ	CC	37						
622.4	617.9	ν	rg2	14	β	rg2	70									
591.7	604.5	β	rg1	35	β	CC	22									
568.6	570.0	β	rg2	17	β	CN1	15	β	CC	30						
543.6	541.5	ν	CC	14	β	CC	28									
543.6	539.0	τ	rg1	44	τ	CC	21									
525.7	528.6	ν	rg1	13	β	rg1	12	β	CN1	27	β	CC	24			
516.8	513.7	β	CN2	29	β	CC	22									
516.8	510.4	β	rg1	31	β	CC	11									
479.4	499.1	β	rg1	10	τ	rg2	25	β	CN2	13	τ	CN2	15			
444.3	452.7	τ	rg2	10	β	CN2	23	β	CC	21						
444.3	447.8	τ	rg1	48	τ	CN1	14									
425.3	421.5	β	rg2	15	τ	rg2	33	β	CC	17						
406.7	407.5	τ	rg2	56												
406.7	391.7	β	rg2	23	ν	CN2	10	β	CN2	11	β	CC	17			
406.7	370.7	τ	rg2	41	β	CN1	12	τ	CC	20						
338.9	351.4	β	CN2	12	β	CC	33									
338.9	345.7	τ	CN1	32	β	CC	11	τ	CC	27						
324.3	332.1	β	CN1	10	τ	CN1	14	τ	CC	54						
300.7	306.8	τ	rg2	13	β	CN1	15	β	CC	29						
300.7	305.1	τ	CN1	16	β	CC	15	τ	CC	27						
300.7	301.1	β	CN2	12	β	CC	45	γ	CH	17						

Table 4 (*Continued*)

Frequency (cm^{-1})		Potential energy distribution[a] (%)														
Measured	Calculated															
300.7	280.7	β	CN2	12	β	CC	43	τ	CC	15						
257.4	262.0	β	CC	11	γ	CH	62									
257.4	258.5	β	CC	19	τ	CC	17	γ	CH	31						
257.4	249.4	β	CC	17	τ	CC	18	γ	CH	13	γ	CH	26			
230.6	240.9	β	CC	16	τ	CC	13	γ	CH	41						
230.6	228.9	γ	CH	68												
215.4	222.3	β	CN1	17	γ	CH	44									
215.4	214.2	β	CC	21	γ	CH	39									
215.4	208.8	β	CC	41	γ	CH	38									
198.2	188.7	τ	rg2	20	β	CC	23	γ	CH	13						
186.2	177.3	β	rg2	13	τ	CN2	11	ν	CC	13	β	CC	17	τ	CC	19
159.6	152.0	β	CC	23	τ	CC	31									
151.6	144.2	τ	CC	56												
145.0	137.8	τ	CN2	13	τ	CC	44									
135.4	128.2	τ	rg1	11	τ	CN1	37	τ	CC	20						
113.0	107.1	τ	rg1	15	β	CC	10	τ	CC	31						
96.7	91.7	τ	rg2	13	τ	CN2	13	β	CC	13	τ	CC	43			
80.5	76.4	τ	CN2	17	τ	CC	58									
73.0	69.2	τ	CN2	37	β	CC	10	τ	CC	39						
61.0	57.9	τ	CN2	43	β	CC	17	τ	CC	32						
52.9	50.2	τ	CN2	15	β	CC	10	τ	CC	62						
46.1	43.8	τ	CC	78												
31.0	29.6	β	CC	47	τ	CC	22									
20.8	19.7	τ	rg2	21	τ	CN2	16	τ	CC	58						
17.5+	16.6	τ	rg2	47	τ	CC	38									

[a] Distributions not less than 10%; ν: stretching; β: in-plane deformation; g: out-of-plane deformation; τ: torsion; rg1:benzene ring in indolene; rg2: the other aromatic ring; N1=N10; N2=N20 (Fig. 2). The mean deviation between the measured and calculated frequencies is 6.78 cm^{-1} and 1.18%.

1620–1500 cm^{-1} range two vibrational modes contain about 50 PED% the νrg1 stretching coordinates (measured frequencies 1601.3 and 1573.4 cm^{-1}), and similarly two have about 50 PED % νrg2 stretching modes (measured frequencies 1614.7 and 1514.4 cm^{-1}). There are not characteristic vibrational modes for CN1 and CN2 type stretchings. These stretching coordinates participate by 10–25 PED% in some vibrational modes.

Table 5 contains the calculated fundamental frequencies for the DPPTVI cation in aqueous solution. For comparison similar results for the isolated cation are also shown. The deviations from the isolated cation frequencies are mostly towards lower frequencies. In the region of the CH stretchings these deviations are 30–40 cm^{-1}, in the mentioned region of the *rg* stretchings the frequencies decease by about 20 cm^{-1}. In general, the weights of PED contribution of the ring stretching coordinates decreased. The νrg1 contribution decreased by 17% at the calculated frequency of 1569.9 cm^{-1} frequency, and the νrg2 contribution – by 8% at the frequency of 1440.9 cm^{-1}. In case of the frequencies 1593.2 cm^{-1} and 1556.1 cm^{-1} this decrease was small, only 3% and 1% for νrg2 and νrg1, respectively (see also Table 4).

4.5. Vibrational spectra

The measured and simulated infrared spectra are presented in Fig. 3. The intense and more or less characteristic bands are marked. The resolution of the most intense band showed that the 1514.4 and 1524.0 cm^{-1} bands overlap in the experimental spectrum (see Table 3 and Figs. 3 and 4). The features in the simulated infrared spectrum differ in intensity and width from the experimental one. The reason is the difference in the conditions. Namely, the experimental spectra were measured in solid state, in chemical environment. The quantum chemical calculations refer to isolated molecule or to aqueous solution (PCM), and are based on the scaled computed frequencies and the calculated infrared intensities for the normal modes. Besides, the simulated spectra were calculated with constant band width for all normal modes.

The measured and simulated Raman spectra are introduced in Fig. 4. The quantum chemically calculated Raman intensities (S_i) were corrected for the excitation wavelength of the experimental spectrum, according to [33]. The equation for the frequency of *i*th vibrational mode (ν_i) has the following form:

$$I_i = f\frac{(\nu_0 - \nu_i)^4}{\nu_i\,[1 - \exp(-(hc\nu_i/kT))]}S_i$$

with excitation frequency ν_0 (in our case corresponding to λ = 785 nm), temperature T (here 293 K), Planck constant h, Boltzmann constant k and speed of light in vacuum c; f is an arbitrary constant valid for all vibrational frequencies of the molecule. This correction bring the calculated spectra closer to the measured ones, however, other problems are similar to those mentioned for the infrared spectra.

The low sensitivity of the applied CCD detector in the NIR region causes the very low SNR over 2000 cm^{-1}. Here the deviations in intensities between the experimental and calculated spectra are greater than in case of the IR spectra.

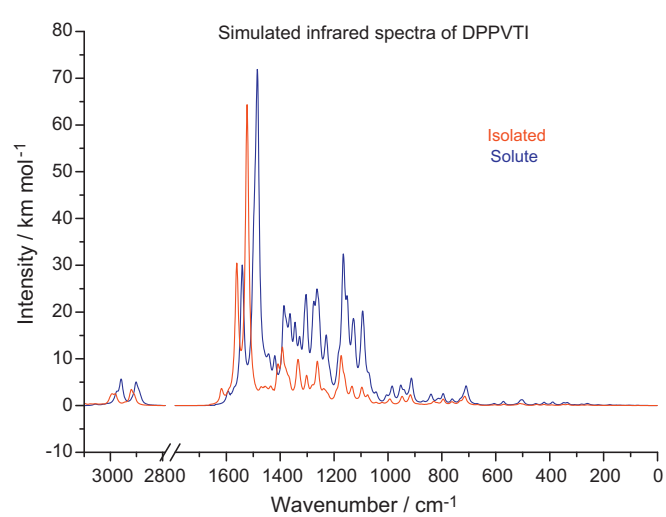

Fig. 5. Comparison of the simulated infrared spectra of the isolated and the solute DPPVTI.

Table 5
Properties of vibrational modes of the DPPTVI cation in aqueous solution.

Frequency (cm^{-1})		Potential energy distribution[c] (%)											
Calculated[a]	Calculated[b]												
3099.0	3059.9	ν	CH	97									
3094.8	3058.3	ν	CH	99									
3077.6	3050.5	ν	CH	99									
3068.8	3027.4	ν	CH	99									
3059.8	3018.2	ν	CH	99									
3057.9	3013.4	ν	CH	99									
3054.9	3008.5	ν	CH	99									
3050.7	2998.2	ν	CH	99									
3043.7	2997.7	ν	CH	99									
3039.1	2989.0	ν	CH	99									
3029.7	2985.8	ν	CH	99									
3003.3	2982.8	ν	CH	98									
3002.5	2980.7	ν	CH	98									
3001.9	2976.8	ν	CH	99									
2999.1	2976.1	ν	CH	99									
2996.3	2974.0	ν	CH	99									
2993.9	2970.2	ν	CH	99									
2992.9	2960.3	ν	CH	99									
2990.7	2960.2	ν	CH	99									
2981.4	2956.7	ν	CH	99									
2979.1	2955.4	ν	CH	99									
2970.9	2945.2	ν	CH	99									
2948.4	2926.4	ν	CH	99									
2943.8	2915.3	ν	CH	98									
2923.5	2911.8	ν	CH	99									
2921.5	2902.3	ν	CH	98									
2919.3	2902.0	ν	CH	97									
2918.7	2899.7	ν	CH	99									
2916.6	2899.6	ν	CH	99									
2910.5	2892.6	ν	CH	99									
2908.4	2890.3	ν	CH	97									
2907.1	2887.9	ν	CH	99									
2906.3	2883.3	ν	CH	91									
1618.2	1593.2	ν	rg2	49	ν	CC	15	β	CH	21			
1586.8	1569.9	ν	rg1	40	β	rg1	23	β	CN1	12	β	CH	13
1575.6	1556.1	ν	rg1	53	β	CC	18	β	CH	14			
1560.5	1539.8	ν	rg1	10	ν	rg2	12	ν	CC	28	β	CH	35
1522.7	1497.9	ν	rg2	26	ν	CN2	16	β	CH	30			
1514.6	1490.9	ν	rg2	41	β	rg2	12	β	CH	22			
1506.3	1483.2	β	CN1	13	ν	CC	20	β	CC	17	β	CH	27
1472.9	1472.8	β	CH	16	β	CH	25	γ	CH	42			
1470.4	1464.0	β	CH	12	β	CH	19	γ	CH	59			
1461.3	1458.8	β	CH	20	γ	CH	54						
1458.4	1457.7	β	CH	22	γ	CH	66						
1456.2	1454.9	β	CH	19	γ	CH	63						
1454.4	1453.5	β	CH	17	γ	CH	63						
1453.7	1452.2	β	CH	25	γ	CH	67						
1452.8	1450.7	β	CH	24	γ	CH	65						
1451.1	1450.0	β	CH	20	γ	CH	78						
1448.1	1444.6	β	CH	18	γ	CH	63						
1446.5	1443.3	β	CH	10	γ	CH	70						
1445.0	1439.5	β	rg2	12	β	CH	14	γ	CH	59			
1438.7	1439.0	β	CH	16	γ	CH	73						
1435.5	1436.3	β	CH	12	γ	CH	75						
1434.5	1433.9	β	CH	18	γ	CH	81						
1430.8	1428.6	ν	rg1	22	β	CH	35	γ	CH	13			
1430.4	1418.8	ν	rg1	32	β	CH	46						
1409.2	1403.0	β	CH	60									
1392.2	1386.2	β	CH	55	γ	CH	10						
1379.5	1377.0	β	CH	86									
1373.5	1370.6	β	CH	84									
1370.2	1366.1	β	CH	97									
1366.5	1361.6	β	CH	58									
1350.2	1354.3	β	CH	99									
1347.4	1344.0	β	CH	57	γ	CH	22						
1337.9	1334.1	β	CH	62	γ	CH	23						
1333.8	1327.1	β	CH	72	γ	CH	12						
1331.0	1315.1	ν	rg2	35	β	CH	10						
1324.5	1309.4	ν	rg1	44	ν	CN1	10	β	CH	15			
1302.2	1302.2	β	CH	58									
1283.6	1282.2	β	CH	60	γ	CH	10						
1278.9	1278.8	β	CH	71	γ	CH	21						
1271.4	1274.7	ν	CC	13	β	CH	59						
1270.0	1263.4	ν	rg1	14	ν	CN1	18	β	CH	44			

Table 5 (*Continued*)

Frequency (cm^{-1})		Potential energy distribution[c] (%)														
Calculated[a]	Calculated[b]															
1261.8	1255.9	ν	rg1	10	ν	CC	31	β	CH	33						
1254.6	1251.9	β	CH	55	γ	CH	19									
1238.8	1237.8	β	CH	63	γ	CH	15									
1231.0	1230.2	ν	rg2	16	β	CH	52									
1226.6	1226.9	β	CH	53	γ	CH	16									
1221.1	1215.2	β	rg1	12	ν	CC	33	β	CH	28	γ	CH	10			
1191.3	1182.8	ν	rg1	12	ν	CC	30	β	CH	33						
1173.7	1165.5	ν	rg2	12	β	CH	55									
1168.8	1163.4	ν	CN2	19	β	CH	35	γ	CH	19						
1160.8	1150.0	ν	rg1	10	ν	CC	19	β	CH	26						
1137.9	1130.3	β	CH	12	β	CH	33	γ	CH	16						
1132.8	1123.6	ν	rg1	20	β	CH	75									
1118.0	1112.0	β	rg2	33	β	CH	30									
1112.5	1102.3	ν	CC	27	β	CH	45	γ	CH	11						
1098.8	1094.1	ν	rg1	23	ν	CC	10	β	CH	42						
1097.2	1089.9	ν	CC	15	β	CH	52									
1090.5	1087.5	ν	rg1	28	β	CH	56									
1083.9	1078.0	ν	CC	22	β	CC	14	β	CH	44						
1075.0	1068.9	ν	CN2	17	ν	CC	10	β	CC	11	β	CH	40			
1067.2	1058.0	ν	CN2	12	ν	CC	31	β	CH	37						
1042.2	1042.8	β	rg1	46	β	CH	22									
1022.1	1005.4	ν	CN2	11	ν	CC	65	β	CH	16						
1008.6	998.3	ν	rg1	16	ν	CN1	16	ν	CC	15	β	CH	31			
1004.3	995.7	β	CH	66	γ	CH	14									
993.4	988.0	ν	CC	74	β	CH	14									
987.8	983.2	ν	rg1	55	ν	CC	10	β	CH	16						
963.4	959.5	ν	rg2	54	β	rg2	24	β	CH	18						
956.0	952.1	γ	CH	89												
950.0	949.6	γ	CH	84												
947.4	939.0	ν	rg2	12	ν	CN2	25	β	CH	24						
921.9	926.6	γ	CH	83												
919.8	923.2	γ	CH	84												
917.7	918.6	ν	CC	30	β	CH	53	γ	CH	12						
915.8	912.3	ν	CC	21	β	CC	19	β	CH	19	γ	CH	10			
907.4	905.9	γ	CH	87												
890.1	884.0	ν	CC	31	β	CC	27	β	CH	15						
875.2	869.0	ν	CC	31	β	CH	33	γ	CH	14						
860.7	858.4	ν	CC	16	β	CH	38	γ	CH	29						
848.0	845.9	ν	CC	13	β	CH	33	γ	CH	24						
836.6	839.2	γ	CH	89												
831.0	836.1	γ	CH	96												
828.5	817.9	ν	CC	60	γ	CH	11									
817.2	811.2	ν	rg2	34	β	rg2	16	ν	CC	23						
794.6	793.9	γ	CH	83												
763.7	768.4	γ	CH	97												
762.7	761.2	β	CH	22	γ	CH	37									
755.1	749.7	ν	rg1	13	β	rg1	21	ν	CN1	14	ν	CC	18	β	CC	12
733.3	731.2	τ	rg1	10	γ	CH	77									
719.9	719.0	τ	rg1	56	τ	CC	14	γ	CH	11						
717.5	718.3	β	CH	23	γ	CH	60									
713.5	709.4	β	rg1	16	β	rg2	10	ν	CN2	13	β	CC	14			
702.4	701.5	τ	rg2	74												
689.0	685.7	β	rg1	30	β	rg2	11	ν	CN2	11	ν	CC	18	β	CC	10
668.3	667.7	τ	rg1	17	τ	rg2	14	τ	CC	38						
617.9	618.8	ν	rg2	14	β	rg2	69									
604.5	605.1	β	rg1	36	β	CC	22									
570.0	570.9	β	rg2	18	β	CN1	12	β	CC	29						
541.5	540.9	τ	rg1	45	τ	CN1	10	τ	CC	22						
539.0	537.5	ν	CC	18	β	CC	32									
528.6	525.4	ν	rg1	18	β	CN1	30	β	CC	20						
513.7	512.3	β	CN2	30	β	CC	25									
510.4	506.9	β	rg1	17	τ	rg2	18	τ	CN2	13	β	CC	10			
499.1	499.0	ν	rg1	10	β	rg1	14	τ	rg2	19	β	CN2	12			
452.7	453.2	β	CN2	24	β	CC	22									
447.8	450.2	τ	rg1	48	τ	CN1	14									
421.5	420.2	β	rg2	15	τ	rg2	35	β	CC	16						
407.5	407.8	τ	rg2	53	β	CC	10									
391.7	387.7	β	rg2	20	ν	CN2	13	β	CN2	11	β	CC	16			
370.7	369.3	τ	rg2	40	β	CN1	11	τ	CC	19						
351.4	349.1	β	CN1	14	β	CC	24	τ	CC	19						
345.7	345.8	τ	CN1	29	β	CC	19	τ	CC	18						
332.1	332.9	β	CN1	12	τ	CN1	14	τ	CC	52						
306.8	308.0	τ	rg2	14	β	CN1	16	β	CC	28						
305.1	306.1	τ	CN1	18	β	CC	19	τ	CC	30						
301.1	299.0	β	CN2	16	β	CC	42	γ	CH	20						

Table 5 (*Continued*)

Frequency (cm^{-1})		Potential energy distribution[c] (%)														
Calculated[a]	Calculated[b]															
280.7	281.0	β	CN2	13	β	CC	44	τ	CC	14						
262.0	264.1	γ	CH	68												
258.5	258.2	β	CC	21	τ	CC	22	γ	CH	20						
249.4	249.8	β	CN2	10	β	CC	19	τ	CC	11	γ	CH	47			
240.9	243.6	β	rg1	10	β	CC	17	τ	CC	11	γ	CH	39			
228.9	228.2	γ	CH	72												
222.3	224.2	γ	CH	64												
214.2	217.7	β	CN1	11	γ	CH	47									
208.8	208.8	β	CC	54	γ	CH	25									
188.7	187.7	τ	rg2	23	β	CC	21	τ	CC	10	γ	CH	13			
177.3	176.1	β	rg2	14	τ	CN2	11	ν	CC	15	β	CC	18	τ	CC	17
152.0	151.6	β	CC	22	τ	CC	31									
144.2	143.5	β	CC	12	τ	CC	54									
137.8	135.5	τ	CN1	15	β	CN2	10	τ	CN2	18	τ	CC	36			
128.2	124.8	τ	rg1	10	τ	CN1	32	τ	CC	29						
107.1	105.3	τ	rg1	18	β	CC	10	τ	CC	32						
91.7	91.7	τ	rg2	11	τ	CN2	13	β	CC	12	τ	CC	47			
76.4	77.3	τ	CN2	18	τ	CC	54									
69.2	71.3	τ	CN2	38	β	CC	10	τ	CC	40						
57.9	56.0	τ	CN2	26	τ	CC	51									
50.2	50.4	τ	CN2	26	β	CC	18	τ	CC	43						
43.8	40.6	τ	CC	80												
29.6	29.8	τ	rg2	12	β	CC	45	τ	CC	22						
19.7	18.6	τ	rg2	20	τ	CN2	18	τ	CC	55						
16.6	15.2	τ	rg2	43	τ	CC	40									

[a] For the isolated DPPTVI cation (for comparison).
[b] For the DPPTVI cation in aqueous solution.
[c] Distributions not less than 10%; ν: stretching; β: in-plane deformation; g: out-of-plane deformation; τ: torsion; rg1: benzene ring in indolene; rg2: the other aromatic ring; N1=N10; N2=N20 (Fig. 2).

The simulated infrared spectra of the isolated and the solute cations are compared in Fig. 5. At the first glance one can observe that most of the bands are shifted towards lower frequencies. This fact as well as the great changes in band intensities below 1400 cm^{-1} are related to the solvent effect. There are several bands in this region with lower or higher contributions of the NC stretching and deformation bands sensitive to the effect of the polar solvent (see Tables 4 and 5).

The simulated Raman spectra of the isolated and solute cations are presented in Fig. 6. Here the low frequency shifts of the bands under the solvent effect are also observable. Besides, changes of a different sort are also revealed. A shoulder 1380 cm^{-1} is resolved in the solution, while the twin peaks near 1270 cm^{-1} merge into one band due to the solvent effect.

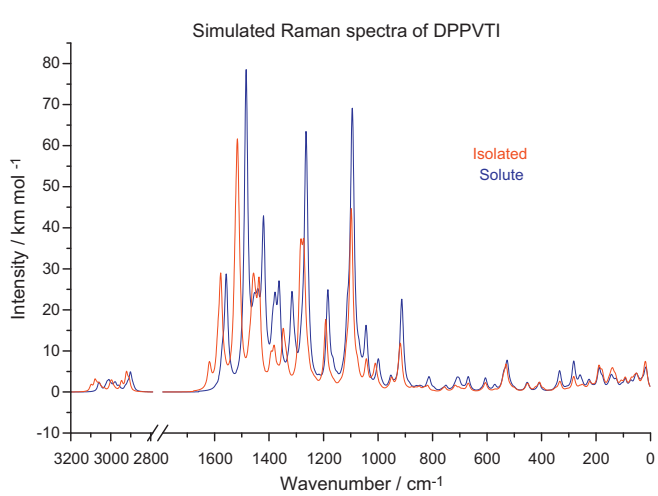

Fig. 6. Comparison of the simulated Raman spectra of the isolated and the solute DPPVTI.

5. Conclusions

The solvent effect on the optimized geometic parameters is small, it is important only in the environment of the nitrogen atoms. The optimized geometry proves the conjugation between the two aromatic systems. In spite of the extended conjugation between the two aromatic rings they are not coplanar.

The solvent effect caused drastic changes in the atomic net charges for several atoms, considering both NBO and Mulliken charges, respectively.

There arose sever problems in the definition of the internal coordinates since the cation contains two aromatic rings without common atom. The force constants reflect the definition of the internal coordinates, their high values point out these difficulties (internal tensions).

The potential energy distributions show the absence of characteristic skeletal vibrational modes. Only ring stretching modes have about 50% contribution. This is also reflected in the experimental and simulated spectra. The solvent effect on the simulated spectra is strong. Both frequency shifts and intensity changes were calculated.

References

[1] T. Deligeorgiev, A. Vasilev, S. Kaloyanova, J.J. Vaquero, Color. Technol. 126 (2010) 55–80.
[2] S.B. Mazzone, N. Mori, M. Burman, M. Palovich, K.E. Belmonte, B.J. Canning, J. Physiol. 575 (2006) 23–35.
[3] S. Xi Chen, W. Barg, Almers, J. Neurosci. 28 (2008) 1894–1903.
[4] Suong-Hoon Kim, Jiang-Zhong Cui, Jin-Yong Park, Eun-Mi Han, Su-Mi Park, Dyes Pigments 59 (2003) 245–250.
[5] S.I. Druzhinin, M.V. Rusalov, B.M. Ushinov, M.V. Alfimov, S.P. Gromov, O.A. Fedorova, Proc. Ind. Sci. (Chem. Sci.) 107 (1995) 721–727.
[6] F. Lehmann, G. Mohr, U.-W. Grummt, Sens. Actuators B 28–39 (1997) 229–234.
[7] A.M. Osman, Z.H. Kahlil, A.I.M. Koraiem, R.M. Abu El-Habd, R.M. Abd El-Aal, Proc. Ind. Acad. Sci. (Chem. Sci.) 109 (1997) 115–134.
[8] S.I. Balogh, M. Ruschak, V. Andruch, F. Billes, Microchim. Acta 166 (2009) 145–150.
[9] V. Andruch, S.I. Balogh, Y.R. Bazel, F. Billes, M. Kádár, R. Karosi, Gy. Parlagh, J. Posta, A. Simon, R. Serbin, M. Torok, Acta Chim. Slov. 54 (2007) 551–557.

[10] A. Feofanov, A. Ianoul, V. Oleinikov, S. Gromov, O. Fedorova, M. Alfimov, I. Nabiev, J. Phys. Chem. 100 (1996) 2154–2160.
[11] E.N. Ushakov, S.P. Gromov, O.A. Fedorova, Y.V. Pershina, M.V. Alfimov, F. Barigelletti, L. Flamigni, V. Balzani, J. Phys. Chem. A 103 (1999) 11188–11193.
[12] A. Feofanov, A. Ianoul, S. Gromov, O. Fedorova, M. Alfimov, I. Nabiev, J. Phys. Chem. B 101 (1997) 4077–4084.
[13] O.A. Fedorova, Y.V. Fedorov, A.I. Vedernikov, S.P. Gromov, O.V. Yescheulova, M.V. Alfimov, M. Woerner, S. Bossmann, A. Braun, J. Saltiel, J. Phys. Chem. A 106 (2002) 6213–6222.
[14] J. Škrlíková, V. Andruch, H. Sklenářová, P. Solich, I.S. Balogh, F. Billes, Anal. Lett., in press.
[15] I.S. Balogh, V. Andruch, M. Kovács, Anal. Bioanal. Chem. 377 (2003) 709–714.
[16] V. Andruch, I.S. Balogh, K. Florián, M. Matherny, Anal. Sci. 16 (2000) 973–974.
[17] R. Shkumbatiuk, Y.R. Bazel, V. Andruch, M. Török, Anal. Bioanal. Chem. 382 (2005) 1431–1437.
[18] S.I. Balogh, V. Andruch, M. Kádár, F. Billes, J. Posta, E. Szabová, Int. J. Environ. Anal. Chem. 86 (2009) 449–459.
[19] M. Kádár, Budapest University of Technology and Economics, private communication.
[20] A.D. Becke, Chem. Phys. 98 (1993) 5648.
[21] C. Lee, W. Young, R.G. Parr, Phys. Rev. B 37 (1988) 785–789.
[22] M.J. Frisch, G.W. Trucks, H.B. Schlegel, G.E. Scuseria, M.A. Robb, J.R. Cheeseman, J.A. Montgomery Jr., T. Vreven, K.N. Kudin, J.C. Burant, J.M. Millam, S.S. Iyengar, J. Tomasi, V. Barone, B. Mennucci, M. Cossi, G. Scalmani, N. Rega, G.A. Petersson, H. Nakatsuji, M. Hada, M. Ehara, K. Toyota, R. Fukuda, J. Hasegawa, M. Ishida, T. Nakajima, Y. Honda, O. Kitao, H. Nakai, M. Klene, X. Li, J.E. Knox, H.P. Hratchian, J.B. Cross, C. Adamo, J. Jaramillo, R. Gomperts, R.E. Stratmann, O. Yazyev, A.J. Austin, R. Cammi, C. Pomelli, J.W. Ochterski, P.Y. Ayala, K. Morokuma, G.A. Voth, P. Salvador, J.J. Dannenberg, V.G. Zakrzewski, S. Dapprich, A.D. Daniels, M.C. Strain, O. Farkas, D.K. Malick, A.D. Rabuck, K. Raghavachari, J.B. Foresman, J.V. Ortiz, Q. Cui, A.G. Baboul, S. Clifford, J. Cioslowski, B.B. Stefanov, G. Liu, A. Liashenko, P. Piskorz, I. Komaromi, R.L. Martin, D.J. Fox, T. Keith, M.A. Al-Laham, C.Y. Peng, A. Nanayakkara, M. Challacombe, P.M.W. Gill, B. Johnson, W. Chen, M.W. Wong, C. Gonzalez, J.A. Pople, Gaussian 03, Revision C.02, Gaussian, Inc., Wallingford, CT, 2004.
[23] S. Miertus, J. Tomasi, Chem. Phys. 65 (1982) 239.
[24] V. Barone, M. Cossi, J. Tomasi, J. Chem. Phys. 107 (1997) 3210.
[25] R. Cammi, B. Menucci, J. Tomai, J. Phys. Chem. A103 (1999) 9100.
[26] GRAMS/386, Galactic Industries Corporation, 1991–1993.
[27] http://www.science.uwaterloo.ca/~cchieh/cact/cact.html.
[28] http://www.ccdc.cam.ac.uk/free_services/teaching/ACS%20symposium/66_Guy_Crundwell.pdf.
[29] R.S. Mulliken, J. Chem. Phys. 23 (1955) 1833.
[30] A.E. Reed, R.B. Weinstock, F.J. Weinhold, J. Chem. Phys. 83 (1985) 735.
[31] A.E. Reed, F.J. Weinhold, L.A. Curtiss, Chem. Rev. 88 (1988) 899.
[32] G. Fogarasi, X. You, P.W. Taylor, P. Pulay, J. Am. Chem. Soc. 114 (1992) 8191–8201.
[33] G. Keresztury, S. Holly, G. Besenyei, J. Varga, A. Wang, J.R. Durig, Spectrochim. Acta Part A 49 (1993) 2007.